REAL-TIME SIMULATION FOR ROBUST CONTROL APPLIED TO ASYNCHRONOUS 3-PHASE INDUCTION MOTOR BASED ON THE PPI CONTROL

NGUYEN VINH QUAN, MAI THANG LONG*

Faculty of Electronics Technology, Industrial University of Ho Chi Minh City, Viet Nam,

** Corresponding author: maithanglong@iuh.edu.vn*

DOIs: https://www.doi.org/10.46242/jstiuh.v76i4.5536

Abstract. This study proposes the method of real-time simulation for the field-oriented control (FOC) of an asynchronous - phase induction motor (IM) based on the parallel proportional-integral (PPI) technique, to control the motor speed. The proposed control strategy requires two independent direct controllers for flux and current through the 3 level-cascade inverters with the algorithm of carrier phase modulation (PM). In particular, the stator field-oriented vector control (SFOC) will be chosen rather than the rotor field-oriented vector control (RFOC) caused by the requirement of voltage, current and stator resistance parameters. The result of real-time simulation is provided by applying Sim-Power-Systems of Matlab-Simulink software via RT-LAB compiler and the hardware simulation in hardware in loop (HIL) via OPAL-RT for 1-Hp, 1400 rad/s IM motor. These simulation and experimental results show the robustness of the PPI controller in the presence of parameter variation, such as, the Rs and Rr resistances increasing by 2 times, changing of torque and speed with the appearance of disturbances.

Keywords. Rotor-flux-oriented, Stator-flux-oriented, Induction motor, PI control; PPI control.

1 INTRODUCTION

The use of electric motors is constantly increasing in the industrial field, such as electric vehicles, especially AC motors [1]. Squirrel cage rotor motors are one of the most widely used asynchronous motors in various fields, 80% of the motors used worldwide are squirrel cage rotor asynchronous motors [2]. Technological advances in power electronics and control have made the use of this type of motor in the renewable energy field possible. As is known, 90% of the motors used worldwide are asynchronous motors due to their durability, low cost and low maintenance costs. Moreover, these motors are characterized by simple and easy control compared to some other motors [3]. In addition, because this type of motor reduces harmful emissions, it is widely used in the field of electric vehicles.

To achieve high performance, the control algorithm for IM must be robust, have a small steady time and improve the performances of the current, in addition to reducing torque ripple and increasing response time, the maintenance level is also low [4]. The above criteria are among the conditions for selecting a control algorithm for asynchronous motors to achieve high performance and fast response in industrial applications [5]. In the industrial field, several control algorithms have been proposed, the most famous of which are backstepping control [6], FOC control [7, 8], direct torque control (DTC) [9], and sliding mode control (SMC) [10]. Other algorithms are also no less important than the previously mentioned algorithms, such as artificial intelligence, in which fuzzy logic (FLC) [11], artificial neural networks (ANN [12], Particle Swarm Optimization (PSO) [13], and Genetic Algorithms (GA) [14] have also been used to control IMs. These intelligent algorithms have been shown to significantly improve the system characteristics, but the ripple problem still exists in the torque. In addition, the system stability problem still does not exist in the case of changing parameters.

In this paper, a advanced SFOC control scheme is proposed to control the magnetic flux and velocity of IM. The proposed algorithm maintains simplicity and ease of implementation while significantly increasing robustness. In addition, the use of the proposed control scheme also helps to reduce the torque, current and magnetic flux ripples and improve the time response of the system. The proposed control scheme is based on a simple solution of using a parallel PI controller (PPI), in which two PI controllers are used in parallel instead of the classic PI controllers [15, 16] to control the velocity and magnetic flux. In fact, when compared with the PI control-based methods [15, 16], to improve the performance for IM control, these control methods must exploit more different control strategies, which may require more complex control

structures and higher computational burden. In this study, simulation results show that the proposed SFOC-PPI algorithm combining a 3rd order cascade inverter with a PM carrier phase modulation algorithm is more effective than the classic SFOC-PI technique.

The paper is divided into three parts as follows. Part 1 is the introduction. Part 2 presents the main content including choosing the mathematical model for IM and multi-level inverter. Part 3 shows the designing of the control laws SFOC_PI, SFOC_PPI. Part 4 performs simulation verification. And finally, conclusions are drawn in Part 5.

2 SYSTEM DESCRIPTION

2.1 IM model in d-q coordinate system

In the field of control, it is possible to reduce the workload and achieve more accurate results by selecting a mathematical model of the motor, the mathematical model of the three-phase IM motor has been selected and implemented on Matlab/Simulink [17]. To derive the IM model, the Park transformation has been used, the Park transformation has rotated the abc-reference frame into the d-q reference frame, due to the perfect alignment of the rotor flux with the d-axis, which means that the q-axis component of the rotor flux can be taken as zero. These reference voltages are also used to calculate the flux linkages, from which the stator and rotor currents are calculated. These currents are then used to derive the final equations for the torque and velocity. The model of the IM in d-q coordinates can be represented by Ba-razzouk et al -1997 [18], which are respectively expressed as follows.

Stator and rotor voltage equations:

$$\begin{cases} u_{sd} = R_s i_{sd} + \dfrac{d\jmath_{sd}}{dt} - w\jmath_{sq} \\ u_{sq} = R_s i_{sq} + \dfrac{d\jmath_{sq}}{dt} - w\jmath_{sd} \end{cases} \tag{1}$$

$$\begin{cases} 0 = R_r i_{rd} + \dfrac{d\jmath_{rd}}{dt} - (w - w_r)\jmath_{rq} \\ 0 = R_r i_{rq} + \dfrac{d\jmath_{rq}}{dt} - (w - w_r)\jmath_{rd} \end{cases} \tag{2}$$

Stator flux equations:

$$\begin{cases} \jmath_{sd} = L_s i_{sd} + L_m i_{rd} \\ \jmath_{sq} = L_s i_{sq} + L_m i_{rq} \end{cases} \tag{3}$$

Rotor flux equations:

$$\begin{cases} \jmath_{rd} = L_r i_{rd} + L_m i_{sd} \\ 0 = L_r i_{rq} + L_m i_{sq} \end{cases} \tag{4}$$

Dynamics equation for rotor velocity:

$$\frac{dw_r}{dt} = \frac{1}{J}(T_e - Bw_r - T_L) \tag{5}$$

And the expression of the electromagnetic torque of IM as a function of rotor flux and stator current is as follows:

$$T_e = \frac{3M}{2L_r} p(\jmath_{rd} i_{sq} - \jmath_{rq} i_{sd}) \tag{6}$$

in which, the symbols of variables and parameters in the above equations are described in detail as the following Table 1 as:

Table 2: The symbols of variables and parameters.

Variables/Parameters	Description	Variables/Parameters	Description
u_{sq}, u_{sd}	Stator voltages (d – q axis).	w, w_r	Synchronous, Rotor angular velocities.

u_{rq}, u_{rd}	Rotor voltages (d – q axis).	R_s, R_r	Stator, rotor resistances.
i_{sq}, i_{sd}	Stator currents (d – q axis).	L_s, L_r, L_m	Stator, rotor, mutal inductances.
i_{rq}, i_{rd}	Rotor currents (d – q axis).	T_e, T_L	Electromagnetic, load torques.
$\varphi_{sq}, \varphi_{sd}$	Stator fluxes (d – q axis).	p	Pole-pairs.
$\varphi_{rq}, \varphi_{rd}$	Rotor fluxes (d – q axis).	B, J	Friction coeficient, Inertia constant

The equations (1) – (6) represent the dynamic properties of the IM model in d-q coordinates, which will be considered as the necessary basis for exploiting the control laws proposed in Section 3.

2.2 The 3rd order cascade inverter

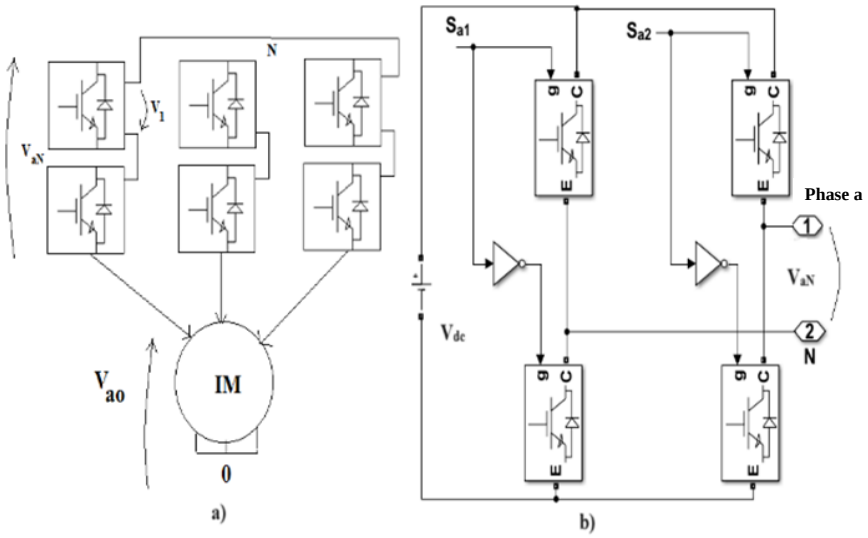

Figure 1: The structure 3rd order cascade inverter (a) and H-bridge for phase a (b).

Fig. 1, shows the 3rd order inverter structure and the H-bridge diagram for one phase consisting of four IGBT (Insulated Gate Bipolar Transistor) switches, we have:

$$\begin{cases} V_{a0} = V_{aN} + V_{N0} \\ V_{N0} = V_{cm} = (V_{aN} + V_{bN} + V_{cN})/3 \end{cases} \quad (7)$$

with V_{cm} is the common-mode voltage (CMV). Let n = 3, which is the number of levels of the inverter, and the Vdc sources are the same, we have a table of the corresponding switches' on/off status for continuous output voltage from [-1Vdc, 0, +1Vdc] as in Table 2.

Table 2: Switching states for phase a.

n	**S_{a1}, S_{a2}**	**Output voltage = (S_{a1} - S_{a2}) V_{dc}**
0	[0, 1]	-1 V_{dc}
1	[0, 0], [1, 1]	0
2	[1, 0]	-1 V_{dc}

Fig. 2 is a PM carrier modulation model for the inverter, with the control signals g(t) and G(t) given by the following equations:

$$G(t) = (g(t) + 1)\frac{n - 1}{2} \quad (8)$$

$$L_X = \begin{cases} n-2, \text{ when } G(t) \geq n-2 \\ fix(G(t)), \text{ when } G(t) < n-2 \end{cases} \quad (9)$$

$$x_X = G(t) - L_X \quad (10)$$

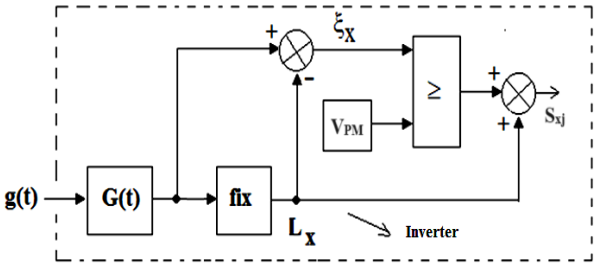

Figure 2: The PM method

The two components of the voltage G(t) are ξx, Lx, where $0 \leq Lx \leq n-2$ is the integer part of the signal G(t), given by equation (9), $0 \leq \xi x \leq 1$ is the remainder after division, given by equation (10), n = 3, is the number of steps of the inverter, Sxj is the state of the key given in Table 1 and V_{PM} is the carrier wave after PM modulation. Consider a high frequency wave with the form of the following equation:

$$e(t) = A_c \cos(w_c t + j), w_c = 2p f_c \quad (11)$$

With $A_c = 1$, the unmodulated carrier wave has the form of equation (12):

$$c(t) = \frac{2}{p}\sin^{-1}(e(t)) = \frac{2}{p}\sin^{-1}(A_c \cos(w_c t + j)) \quad (12)$$

Next, the carrier wave will be normalized as follows:

$$V_C(t) = \frac{\max(c(t)) + c(t)}{\max(c(t)) - \min(c(t))} \quad (13)$$

with max and min being the largest and smallest amplitudes of c(t). And, by considering the control signal:

$$g(t) = E_m \sin(w_m t), w_m = 2p f_m \quad (14)$$

From high frequency waves $e(t)$, if the phase angle j changes according to the control signal $g(t)$, we have PM phase modulation:

$$e_{PM} = A_c \cos\{w_c t + (m_{px} / E_m) g(t)\} \quad (15)$$

with $q = w_c t + (m_{px} / E_m) g(t)$, m_{px} being the phase modulation index, and x = a, b, c. Substituting into equation (12, 13), we have the PM phase modulated carrier. Fig. 3 shows a PM modulated carrier with frequency fc = 1KHz, modulation index m_{px} = 10. We can see that the PM modulated carrier has a phase that contains all the information of the control signal $g(t)$. Fig.4 shows the effects of Em index and carrier frequency fc on the average %THD of phase voltage Vx (x = a, b, c), the average %THD of Vx increases rapidly when increasing carrier frequency fc from 1KHz to 5KHz, increasing Em index from 0 to 1 reduces %THD of Vx. Therefore, Em index and carrier frequency fc will affect the performance of PM modulation algorithm in the entire operating range of the inverter.

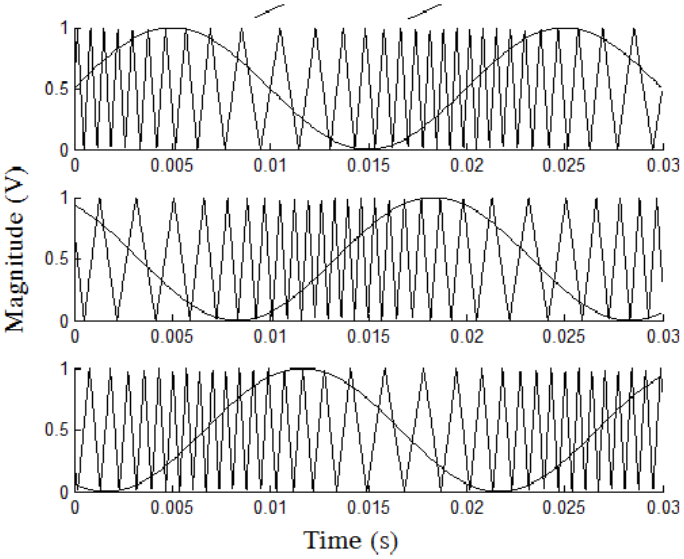

Figure 3: Carrier wave after PM modulation

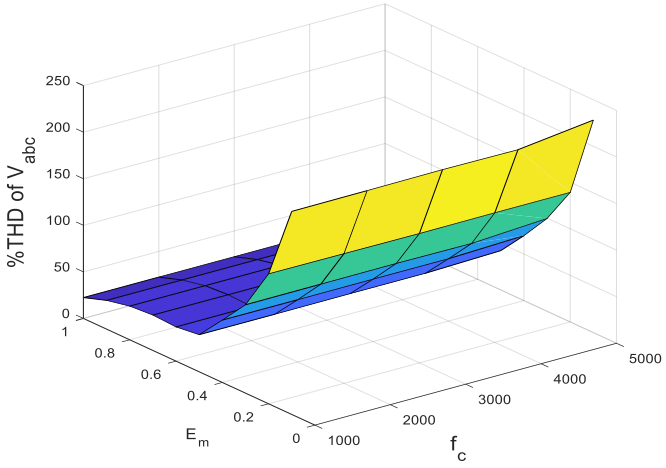

Figure 4: Effect of Em and fc on %THD

3 CONTROL DESIGN

If we choose a reference system attached to the stator flux vector, the angular velocity of the coordinate system is equal to the angular velocity of the stator flux vector and the d-axis of the coordinate system coincides with the stator flux vector, from the equations (1) – (6), it yields:

$$\varphi_{sq} = \dot{\varphi}_{sq} = 0 \tag{16}$$

$$u_{sd} = R_s i_{sd} + \dot{\varphi}_{sd} \tag{17}$$

$$T_e = \frac{3}{2} p(\varphi_{sd} i_{sq}) \tag{18}$$

$$\varphi_{sd} = \int (u_{sd} - R_s i_{sd}) dt \tag{19}$$

The FOC algorithm based on PPI controller is shown in Fig. 5, in which 4 controllers are used to control the motor flux and speed. The FOC algorithm requires two completely independent controllers for flux and velocity, where the flux is estimated from the system of equations (1), as the following results:

$$u_{sd} = R_s i_{sd} + \dot{\varphi}_{sd}, \varphi_{sq} = 0 \Rightarrow \varphi_{sd} = \int (u_{sd} - R_s i_{sd}) dt \tag{20}$$

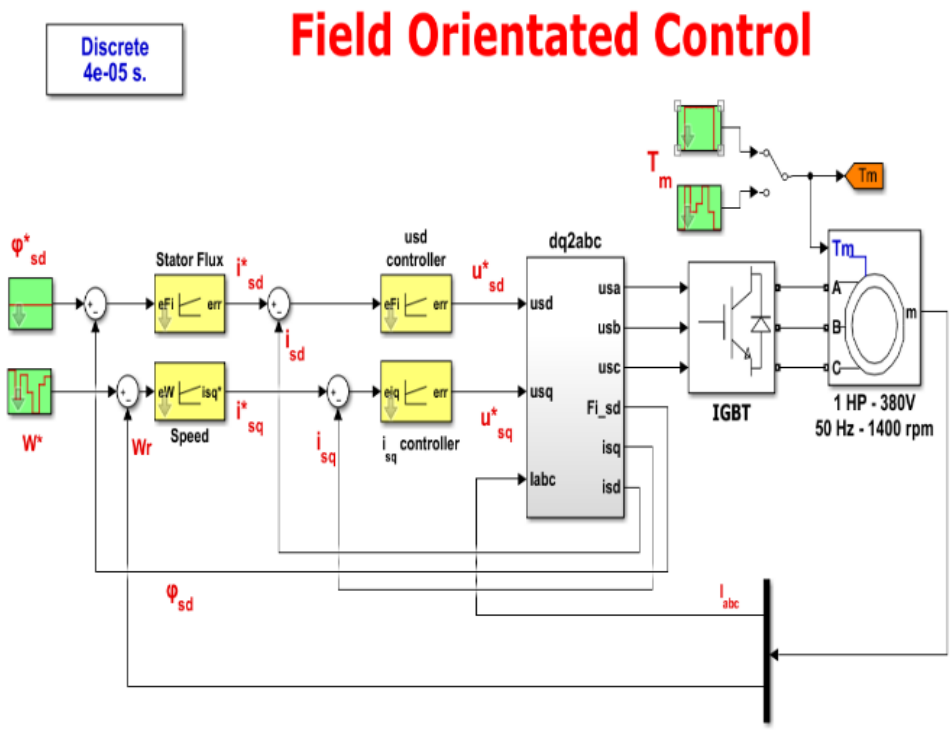

Figure 5: The proposed FOC-PPI control diagram

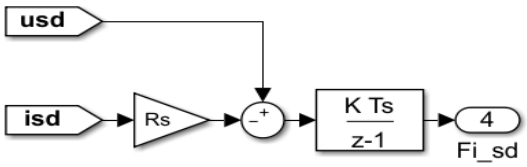

Figure 6: Estimation diagram φ_{sd}

Equation (20) is the mathematical model for estimating the magnetic flux, and Fig.7 is the Simulink diagram for estimating the magnetic flux φ_{sd}. The FOC PI control aims to calculate the reference voltage value based on the error of velocity and magnetic flux. Equations (21) and (22) represent the reference value for each voltage u^*_{sd} and u^*_{sq} [15, 16, 19]:

$$u^*_{sd}(t) = K_1 e_{isd}(t) + K_2 \int_0^t e_{isd}(t)\,dt \tag{21}$$

$$u^*_{sq}(t) = K_1 e_{isq}(t) + K_2 \int_0^t e_{isq}(t)\,dt \tag{22}$$

where $e_{isd} = i^*_{sd} - i_{sd}$ and $e_{isq} = i^*_{sq} - i_{sq}$ are the current errors along the d-q axis, K_1, K_2 are the PI control gains. The desired values for currents i^*_{sd} and i^*_{sq} can be calculated using the following equations as:

$$i^*_{sd}(t) = K_3 e_{\varphi sd}(t) + K_4 \int_0^t e_{\varphi sd}(t)\,dt \tag{23}$$

$$i^*_{sq}(t) = K_3 e_{\omega}(t) + K_4 \int_0^t e_{\omega}(t)\,dt \tag{24}$$

where $e_{\omega} = \omega^* - \omega_r$ and $e_{\varphi sd} = \varphi^*_{sd} - \varphi_{sd}$ are the errors of the stator velocity and flux, respectively. K_3, K_4 are the PI control gains.

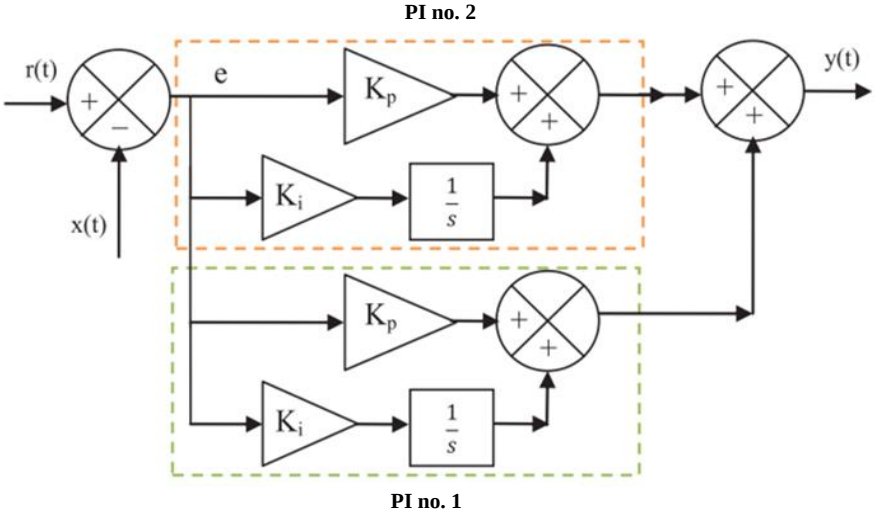

Figure 7: FOC-PPI control diagram

The proposed FOC-PPI algorithm is a modification of the classical algorithm, in which the PI controller is replaced by a PPI controller as shown in Fig. 7, where four PPI controllers are used to control the flux and velocity. The proposed FOC-PPI algorithm still outperforms FOC-PI in terms of results, especially in terms of ripple for the torque and THD value of the stator current, equations (21) to (24) become:

$$u_{sd}^{*}(t) = \left(K_1 e_{isd}(t) + K_2 \int_0^t e_{isd}(t)\,dt\right) + \left(K_1 e_{isd}(t) + K_2 \int_0^t e_{isd}(t)\,dt\right) \quad (25)$$

$$u_{sq}^{*}(t) = \left(K_1 e_{isq}(t) + K_2 \int_0^t e_{isq}(t)\,dt\right) + \left(K_1 e_{isq}(t) + K_2 \int_0^t e_{isq}(t)\,dt\right) \quad (26)$$

$$i_{sd}^{*}(t) = \left(K_3 e_{\varphi sd}(t) + K_4 \int_0^t e_{\varphi sd}(t)\,dt\right) + \left(K_3 e_{\varphi sd}(t) + K_4 \int_0^t e_{\varphi sd}(t)\,dt\right) \quad (27)$$

$$i_{sq}^{*}(t) = \left(K_3 e_{\omega}(t) + K_4 \int_0^t e_{\omega}(t)\,dt\right) + \left(K_3 e_{\omega}(t) + K_4 \int_0^t e_{\omega}(t)\,dt\right) \quad (28)$$

4 SIMULATION RESULTS

Table 3: IM parameters.

Parameters	Values	Parameters	Values
Power	1HP, 50 Hz	J	0.005 (kg.m^2)
Line Voltage	380 (V)	F	0.000503 (N.m.s)
Velocity	1400 (rpm)	DC link	200V$_{dc}$
Torque T_m	5 (N.m)	T_s	40 µs
R_s, L_s	0.087 (Ω), 5 (mH)	Carier frequency f_c	2.5KHz
R_r, L_r	0.228 (Ω) ,1(mH)	Modulation method	PM
p	2	Modulation index m_{px}	2

Simulation results are performed on Matlab/Simulink with sampling time Ts = 40µs, the results are applied to the motor with parameters given in Table 3 combining a 3rd order cascade inverter with PM modulated carrier. The real time simulation process is implemented by HIL techniques incorporating with the OPAL - RT system and cascade inverter [19]. The FOC-PPI control algorithm is modeled on the real-time simulator, the switching states are sent to the physical model of the inverter and motor through the digital ports of the OP8660. Then, the feedback signals, such as stator current, stator voltage, and speed will be sent to the OP4510 through the analog ports of the OP8660. The data obtained on the PC is due to

the interaction with the OP4510.

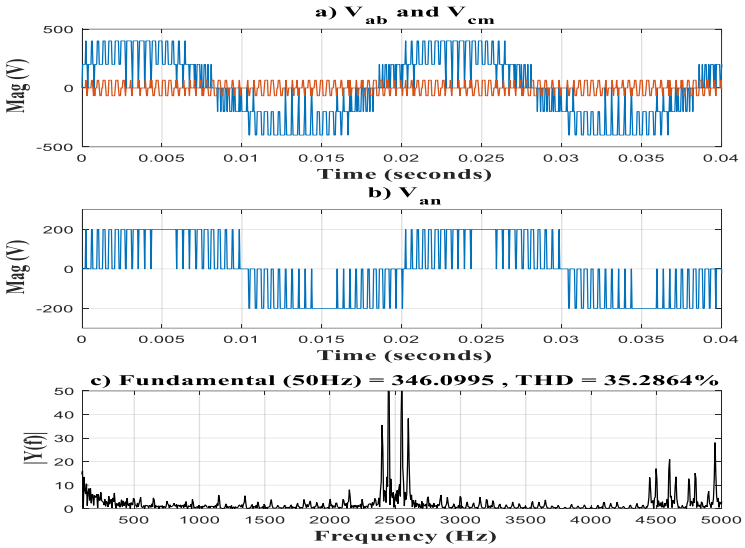

Figure 8: FOC-PPI control diagram

In Fig. 5, we only need to replace the four classic PI controllers with PPI controllers (equations 25-28) to get the SFOC control diagram based on PPI control. Fig. 8a, line voltage Vab, CMV voltage, Fig. 8b phase voltage Van and Fig. 8c is FFT of Vab of 3rd order cascade inverter, with THD = 35.28%. Fig. 9, comparing the control results between the classic SFOC-PI algorithm (red discontinuous curve) and the proposed classic SFOC-PPI algorithm (black curve), shows the results as follows. Fig. 9a, the estimated flux of IM when using the classic PI controller is overshooting, with a large settling time of about 0.2 seconds, while the controller with PPI algorithm has the estimated flux closely following the desired flux and has a small settling time of about 0.1 seconds. Fig. 9b, the measured velocity of IM when using the classic PI controller fluctuates around the set velocity, while the controller with PPI algorithm has the measured velocity closely following the set velocity and has a settling time of about 0.2 seconds.

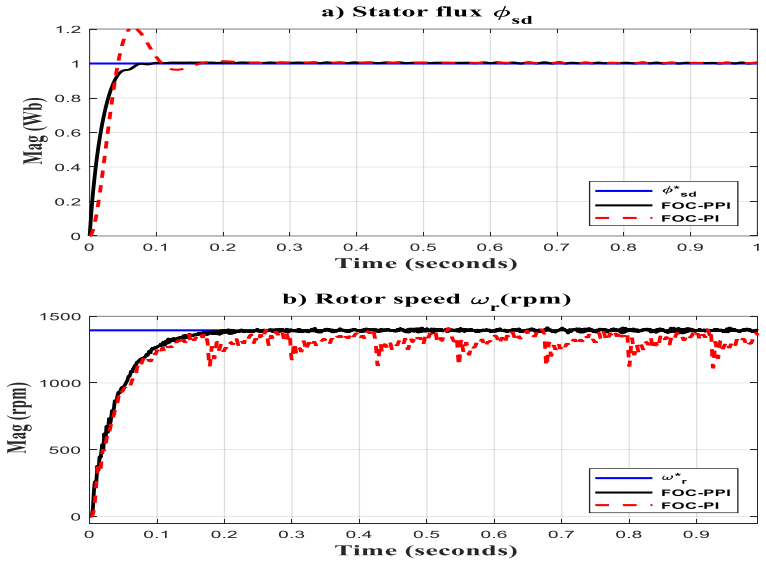

Figure 9: a) Magnetic flux of FOC-PPI and FOC-PI. b) Velocity of FOC-PPI and FOC-PI.

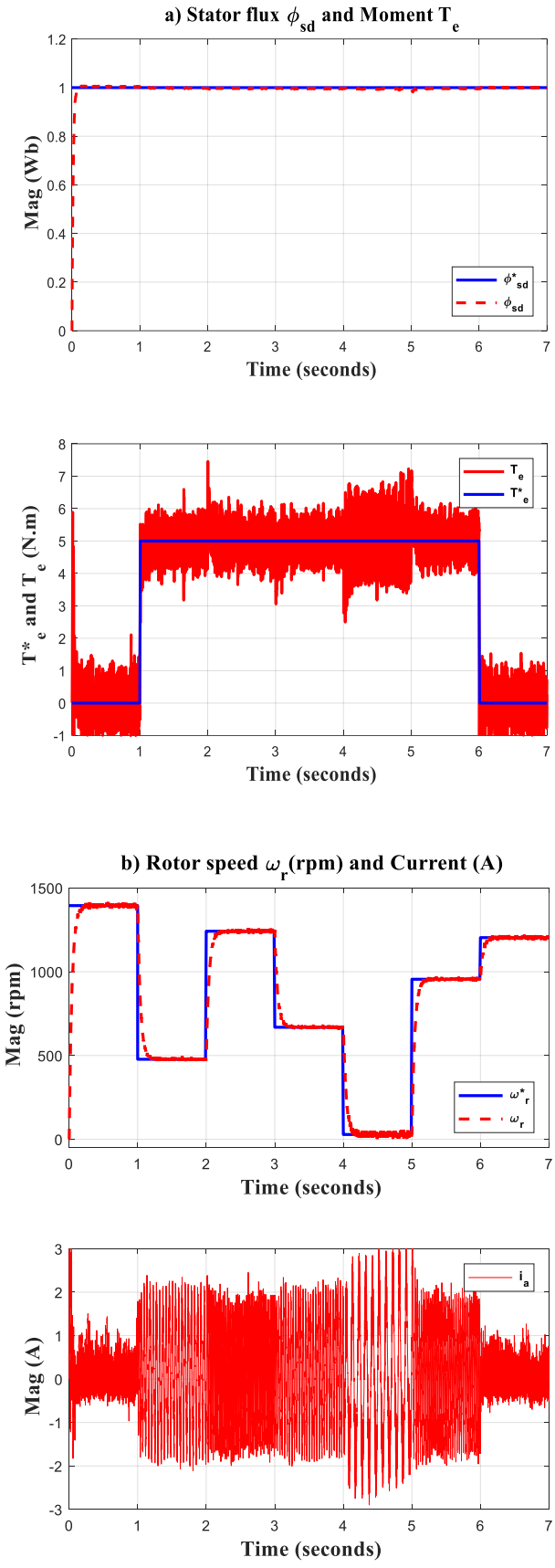

Figure 10: a) Magnetic flux φ_{sd} and torque Te. b) Velocity ω_r and current i_{sa}.

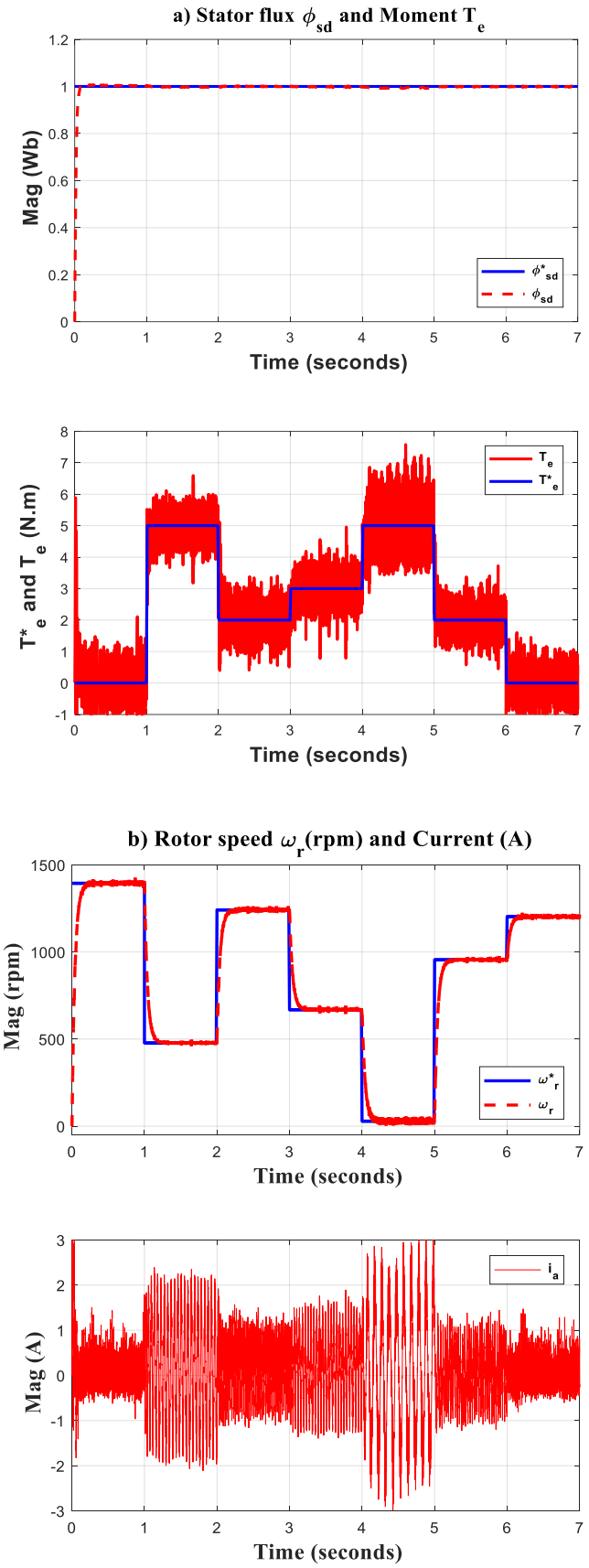

Figure 11: a) Magnetic flux φ_{sd} and torque Te. b) Velocity ω_r and current i_{sa}.

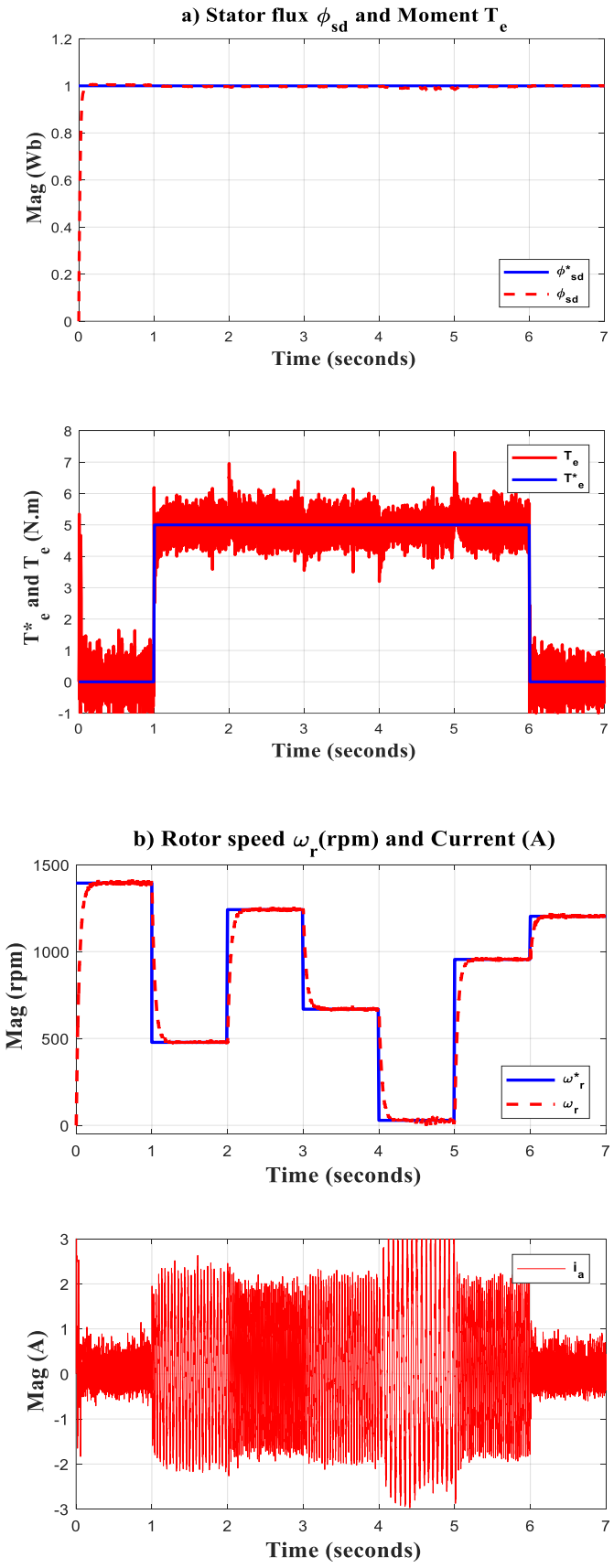

Figure 12: a) Magnetic flux φ_{sd} and torque Te. b) Velocity ω_r and current i_{sa} .

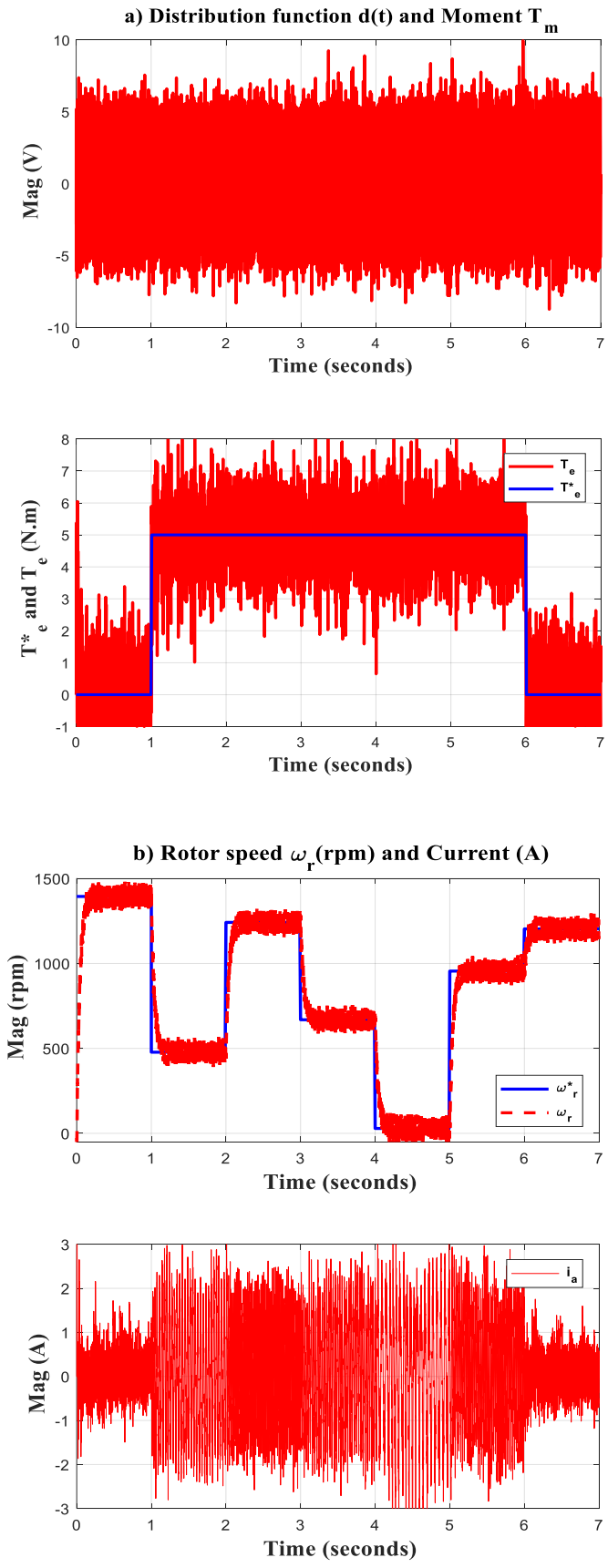

Figure 13: a) Noises and torque Te. b) Velocity ω_r and current i_{sa} .

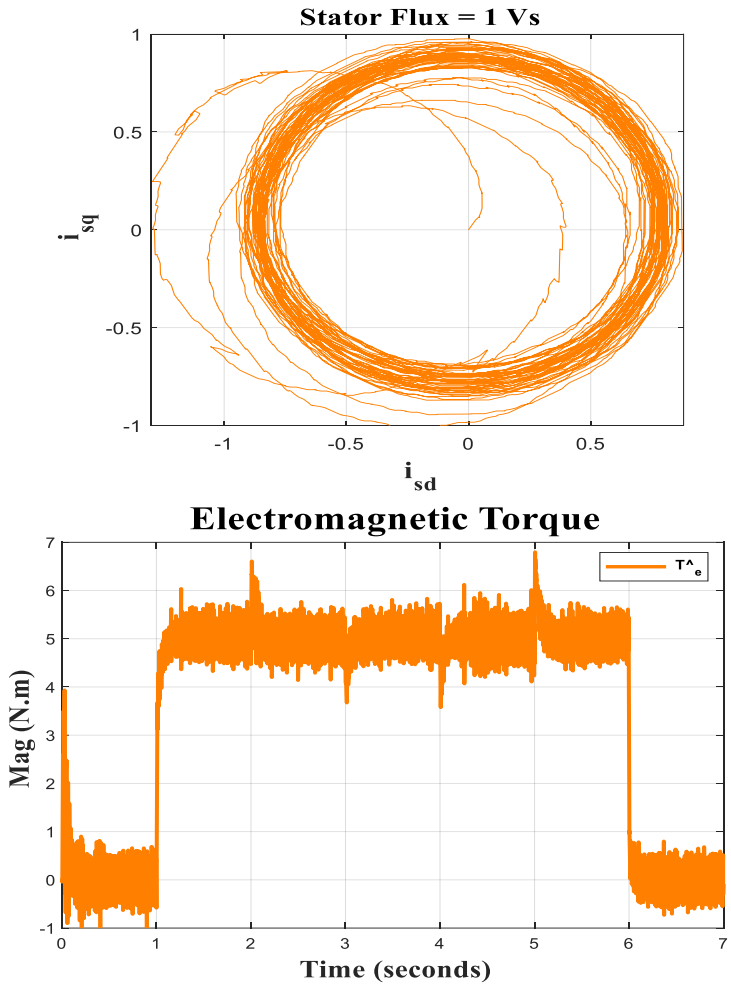

Figure 14: Simulation for stator flux vector and moment.

Fig. 10a shows that when the speed changes, the desired flux φ_{sd}^{*} and the estimated flux φ_{sd} coincide, the torque Te is overshooting at the lowest speed of 20 rpm. Fig. 10b shows that the phase current a reaches a value of about 1A at seconds (0,1) and (6,7), at a speed value of 20 rpm the current reaches nearly 3A, the measured speed ω_r follows the set speed ω_r^{*} well from the maximum value of 1400 rpm to the lowest value of 20 rpm and, fluctuates slightly at times of rapid change. Fig. 11a, simulation when the torque varies, the applied flux and the estimated flux coincide, at the low velocity point the torque still overshoots. Fig. 11b, the measured speed follows the set speed well, the current phase reaches about 3A at 20 rpm.

Fig. 12a, simulates when the resistance Rs increases by 2 times compared to the initial value, the estimated magnetic flux decreases slightly at the speed value of 20 rpm but still follows the set magnetic flux, the measured torque Te still follows the set torque T*e, Fig. 12b, shows that the phase current a reaches a value of about 3A at the lowest speed value, the measured velocity follows the set velocity well. Fig. 13a, simulates when the resistances Rr and Rs increase by 2 times compared to the initial value, randomly distributed d(t) with amplitude ±7V, the measured torque fluctuates strongly, Fig. 13b, shows that the phase a current reach about 3A, the measured velocity still follows the set velocity well. Fig. 14 shows the stator flux vector φ_s and moment Te when controlling SFOC-PPI for a three-phase asynchronous motor with parameters given in Table 3.

The simulation results show that the magnetic flux and torque are separated and follow the desired values, the motor speed follows the desired speed well from the lowest value of 20 rpm to the highest value of 1400 rpm. For the stability of the PPI controller, it is not much affected when the parameters change such as: the resistance Rs and Rr increase to 2 times the initial value, the torque and speed change with the presence of noise. The simulation results also show that the PPI controller has significantly improved the ripple of the

stator current, torque, response and settling time of the system. In addition, the third-order inverter with PM phase-modulated carrier has reduced the switching frequency of IGBT switches, reduced common mode voltage, reduced harmonics in the stator current and ripple of the torque, leading to increased stability of the PPI controller. As a result, with the results obtained from real-time simulation process, it is clear that under the same operating conditions, the proposed SFOC-PPI algorithm gives better performance than the classic SFOC-PI algorithm. In addition, the results also show that the PPI controller has higher stability than the PI controller when the speed changes and some parameters of the motor (such as stator resistance, rotor) increase with the participation of noise.

5 CONCLUSIONS

The paper presents a method of controlling the stator flux direction for a three-phase squirrel-cage rotor motor based on PPI control. Simulation results show that the flux and torque are separated and follow the set value, the motor speed follows the set speed well from the lowest value of 20 rpm to the highest value of 1400 rpm. The stability of the PPI controller: it is not affected much when the parameters change such as: the resistance Rs and Rr increase to 2 times the initial value, the torque and velocity change with the presence of noise. Simulation results also show that the PPI controller has significantly improved the ripple of the stator current, torque, response and settling time of the system. The third-order inverter with PM phase-modulated carrier has reduced the switching frequency of IGBTs, reduced common mode voltage, reduced harmonics in stator current and torque ripple, leading to increased stability of the PPI controller. With the results obtained from the simulation results, it is clear that under the same operating conditions, IM 1hp-380V, the proposed SFOC-PPI algorithm gives better performance than the classic SFOC-PI algorithm. In addition, the results show that the PPI controller has higher robustness than the PI controller when the speed changes and some motor parameters (such as stator and rotor resistance) increase with the participation of noises.

ACKNOWLEDGMENT

This work was supported by the Industrial University of Ho Chi Minh City, Vietnam. The authors would like to thank the associate editor and the reviewers for their valuable comments.

REFERENCES

[1] P. J. Shaija and A. E. Daniel, *An intelligent speed controller design for indirect vector-controlled induction motor drive system*, Procedia Technology, vol. 25, pp. 801–807, 2016.

[2] A. N. Hussain and A. K. Mohaisen, *Performance improvement of speed control for induction motor by using intelligent optimization technique*, Journal of Theoretical and Applied Information Technology, vol. 95, no. 18, pp. 4913–4921, 2017.

[3] P. Maidana, C. Medina, J. Rodas, E. Maqueda, R. Gregor, P. Wheeler, *Sliding-mode current control with exponential reaching law for a three- phase induction machine fed by a direct matrix converter*, Energies, vol. 15, no. 22, 2022.

[4] I. M. Mehedi, N. Saad, M. A. Magzoub, U. M. Al- Saggaf, A. H. Milyani, *Simulation analysis and experimental evaluation of improved field-oriented controlled induction motors incorporating intelligent controllers*, IEEE Access vol. 10, pp. 18380–18394, 2022.

[5] H. Hadla, F. Santos, *Performance comparison of field-oriented control, direct torque control, and model-predictive control for SynRMs*, Chinese Journal of Electrical Engineering, vol. 8, no. 1, pp. 24–37, 2022.

[6] D. Zellouma, H. Benbouhenni, Y. Bekakra, *Backstepping control based on a third-order sliding mode controller to regulate the torque and flux of asynchronous motor drive*, Periodica Polytechnica Electrical Engineering and Computer Science, vol. 67, no. 1, pp. 10–20, 2023.

[7] F. Xie, W. Qun-jing, L. Gou-li, 2012. Optimization research of FOC based on PSO of induction motors, in *2012 15th International Conference on Electrical Machines and Systems (ICEMS), Sapporo, Japan*, 2012, pp. 1–4.

[8] M. Kuchar, P. Brandstetter and M. Kaduch, Sensorless induction motor drive with neural network, in *2004 IEEE 35th Annual Power Electronics Specialists Conference (IEEE Cat. No.04CH37551), Aachen, Germany*, 2004, pp. 3301-3305.

[9] H. Benbouhenni, *Etude comparative entre la commande DTC neuronale et la commande DTC basée sur le contrôleur PI-neuronale de la machine asynchrone*. Revue Ivoirienne des Sciences et Technologie, vol. 29, pp. 30–43, 2017.

[10] S. Zhao, H. Yu, J. Yu, B. Shan, Induction motor DTC based on adaptive SMC and fuzzy control. in *The 27th Chinese Control and Decision Conference (2015 CCDC), Qingdao, China*, , 2015, pp. 4474–4479.

[11] H. F. Azgomi, J. Poshtan, Induction motor stator fault detection via fuzzy logic, in: *2013 21st Iranian Conference on Electrical Engineering, ICEE, Mashhad, Iran*, 2013, pp. 1–5.

[12] R. Yatsiuk, S. Husach, Research on neural network vector control system for induction motor, in *2020 IEEE Problems of Automated Electrodrive, Theory and Practice, PAEP, Kremenchuk, Ukraine*, 2020, pp. 1–4.

[13] A. K. Singh, D. K. Chaturvedi, N. K. Pal, PSO based fractional order PID controller for speed control of induction motor, in *2019 2nd International Conference on Power Energy, Environment and Intelligent Control, PEEIC, Greater Noida, India*, 2019, pp. 574–576.

[14] M. M. Ismail, Improving the performance of the DTC saturated model of the induction motor in case of two level and three level VSI using GA and PSO algorithms, in *2012 Japan-Egypt Conference on Electronics, Communications and Computers, Alexandria, Egypt*, 2012, pp. 79–84.

[15] P. Mahesh and S. R. Arya, *Randomized Self-Structuring Adaptive Neuro-Fuzzy Based Induction Motor Drives with Optimized FOPI Gains*, CPSS Transactions on Power Electronics and Applications, vol. 9, no. 4, pp. 465-475, 2024.

[16] F. AtaAllah, M. Elsaadany, M. Q. Elahi, S. Mukhopadhyay and H. Rehman, *Nested FOPI and PI Controller Performance Comparison for Electric Vehicle Traction System*, IEEE Access, vol.13, pp. 63310-63323, 2025.

[17] M. Said, D. Aziz, I. Atif, N. E. Ouanjli, *ANT-colony optimization-direct torque control for a doubly fed induction motor: An experimental validation*, Energy Reports, vol. 8, pp. 81–98, 2022.

[18] A. Ba-razzouk, A. Cheriti, G. Olivier, A neural networks-based field-oriented control scheme for induction motors, in *IAS '97. Conference Record of the 1997 IEEE Industry Applications Conference Thirty-Second IAS Annual Meeting, New Orleans, LA, USA*, 1997, vol. 2, pp. 804–811.

[19] Nguyen Vinh Quan, Mai Thang Long, *IMC-PI scalar control method for three-phase asynchronous induction motor with multilevel inverter*, Journal of Electrical Engineering & Technology, 2025. https://doi.org/10.1007/s42835-025-02190-w.

MÔ PHỎNG THỜI GIAN THỰC CHO ĐIỀU KHIỂN BỀN VỮNG ĐỘNG CƠ BA PHA KHÔNG ĐỒNG BỘ TRÊN CƠ SỞ ĐIỀU KHIỂN PPI

NGUYỄN VINH QUAN, MAI THĂNG LONG*

Khoa Công nghệ Điện tử, Đại học Công nghiệp Thành phố Hồ Chí Minh,

** Tác giả liên hệ: maithanglong@iuh.edu.vn*

Tóm tắt. Bài báo này sẽ đề xuất phương pháp mô phỏng thời gian thực cho điều khiển định hướng từ thông FOC động cơ không đồng bộ ba pha IM trên cơ sở điều khiển PPI để điều khiển tốc độ động cơ, yêu cầu hai bộ điều khiển trực tiếp hoàn toàn độc lập nhau cho từ thông và dòng điện thông qua biến tần cascade bậc 3 với giải thuật điều chế pha sóng mang PM, điều khiển định hướng vector từ thông stator SFOC thì được chọn hơn là định hướng vector từ thông rotor RFOC, do bộ điều khiển không phụ thuộc nhiều vào tham số động cơ, bộ điều khiển này yêu cầu các tham số về điện áp, dòng điện, và điện trở stator. Các kết quả mô phỏng trong thời gian thực RT- Real Time, sử dụng SimPowerSystems của matlab-simulink thông qua trình biên dịch RT-LAB, giải thuật mô phỏng phần cứng trong vòng lặp HIL- Hardware-in-the-Loop bởi thiết bị OPAL-RT cho động cơ 1-hp, 1400-rad/s loại rotor lồng sóc, kết hợp biến tần cascade bậc ba với giải thuật điều chế pha sóng mang PM, cho thấy tính bền vững của bộ điều khiển PPI, bộ điều khiển không chịu nhiều tác động khi các tham số thay đổi như: điện trở Rs và Rr tăng đến 2 lần giá trị ban đầu, mô-men và vận tốc biến thiên cùng với sự hiện diện của nhiễu.

Từ khóa. Định hướng từ thông rotor, Định hướng từ thông stato, Động cơ từ cảm, Điều khiển PI; Điều khiển PPI.

Ngày gửi bài: 25/12/2024

Ngày chấp nhận đăng: 07/5/2025